Geochemistry of the Cretaceous–Tertiary boundary at Blake Nose (ODP Leg 171B)

F. MARTÍNEZ-RUIZ[1], M. ORTEGA-HUERTAS[2], D. KROON[3], J. SMIT[4], I. PALOMO-DELGADO[2] & R. ROCCHIA[5]

[1]*Instituto Andaluz de Ciencias de la Tierra, CSIC-Universidad de Granada, Facultad de Ciencias, Avda. Fuentenueva s/n, 18002 Granada, Spain (e-mail: fmruiz@goliat.ugr.es)*

[2]*Departamento de Mineralogía y Petrología, Facultad de Ciencias, Universidad de Granada, Avda. Fuentenueva s/n, 18002 Granada, Spain*

[3]*Department of Geology and Geophysics, University of Edinburgh, Grant Institute, West Mains Road, Edinburgh EH9 3JW, UK*

[4]*Department of Sedimentary Geology, Vrije Universiteit, 1081 HV Amsterdam, Netherlands*

[5]*Centre des Faibles Radioactivités, Laboratoire CEA–CNRS, 91198 Gif-sur-Yvette Cedex, France*

Abstract: The Cretaceous–Tertiary (K–T) boundary at Blake Nose, in the NW Atlantic, is recorded by a coarse, poorly graded and poorly cemented layer mostly consisting of green spherules that are mainly composed of smectite. Geochemical patterns across the boundary are governed by the source material of the spherule bed and postdepositional processes. The chemical composition and the nature of this bed indicate that it derived from melted target rocks from the Chicxulub impact structure. Ir and other typical extraterrestrial elements do not present significant enrichments, which suggests that the spherule bed material derived from crustal rocks. Ir instead reaches its highest concentration in the burrow-mottled calcareous ooze above the spherule bed, suggesting that it is associated to the finest fraction deposited after the target-rock-derived material. Only the Ni and Co content show slight enrichments within the upper part of the spherule layer, although most of the trace element profiles resulted from diagenetic alteration. During the alteration of glass to smectite, the concentrations of certain trace elements, such as the rare earth elements, were severely changed. In addition, oxygen-poor conditions also led to the remobilization of redox-sensitive elements, which show enhanced concentration at the top or above the spherule bed. Diagenetic remobilization may have also affected the Ir concentration.

Since Alvarez *et al.* (1980) first proposed a meteorite impact as the probable cause of the mass extinction at the end of the Cretaceous period, several lines of evidence have been used to support this model, one of the main arguments being the enhanced concentration of typical extraterrestrial elements in the boundary material, such as Ir and other platinum-group elements (PGE). These elements have been sought in sediments from this age to constrain the boundary in relation to the faunal turnover. In the last two decades, Ir anomalies at the Cretaceous–Tertiary (K–T) boundary have been found at many K–T sites throughout the world. In addition to the PGEs, anomalous concentrations of other chemical elements have also been reported in the boundary sediments (e.g. Kyte *et al.* 1980, 1985; Schmitz 1985; Strong *et al.* 1987; Zachos *et al.* 1989; Smit 1990; Martínez-Ruiz *et al.* 1992; Bhandari *et al.* 1993). The vast literature on this topic prevents our mentioning all the sites and geochemical anomalies reported thus far, although all the data published until now provide consistent evidence supporting first the extraterrestrial hypothesis (in the 1980s) and later also the impact site at the Chicxulub crater (e.g. Hildebrand *et al.* 1991; Koeberl & Sigurdsson 1992, Sharpton *et al.* 1993; Smit 1999). Despite all the advances made in the knowledge of this devastating impact and its environmental consequences, more work is undeniably needed for complete understanding. Ocean Drilling Program (ODP) Leg 171B contributed a substantial

From: KROON, D., NORRIS, R. D. & KLAUS, A. (eds). 2001 *Western North Atlantic Palaeogene and Cretaceous Palaeoceanography.* Geological Society, London, Special Publications, **183**, 131–148.
0305-8719/01/$15.00

advance in this field by adding a new site (Blake Nose, NW Atlantic) offering the possibility of studying the composition of the Cretaceous, Tertiary and K–T boundary sediments in a succession recording the mass extinction and the proximal ejecta fallout from the Chicxulub crater, and providing also further evidence for a bolide impact at Chicxulub (Norris *et al.* 1998), sometimes questioned in the literature (e.g. Keller *et al.* 1993). Cretaceous and Tertiary boundary sediments recovered by ODP Leg 171 at Blake Nose are similar to those from other marine K–T sections in the North Atlantic margin (Klaver *et al.* 1987; Olsson *et al.* 1997), with the exception of the remarkable thickness of the spherule bed at Site 1049. The thickest bed (17 cm) was recovered at Hole 1049A, whereas at Holes 1049B and 1049C it is around 9 cm thick. The variable thickness of the spherule bed at the three holes drilled at this site, as well as the presence of Cretaceous foraminifera and Cretaceous clasts in the spherule bed, point to reworking of the spherule bed material (Norris *et al.* 1999; Klaus *et al.* 2000). Despite the absence of a precise stratigraphy, its geochemical composition is evidence of the nature of the impact-generated material and further supports the Chicxulub impact model. The main focus of this paper is therefore to study the geochemical anomalies from Blake Nose sediments to constrain the terrestrial–extraterrestrial contribution at this location, the patterns for extraterrestrial material distribution, as well as the chemical element distribution associated with the impact event.

Samples and analytical methods

Samples from the K–T boundary interval at Holes 1049A, 1049B, 1050C and 1052E, Blake Nose (NW Atlantic) (Fig. 1), were analysed for major and trace element concentrations. In the studied interval, a spherule bed occurs at the biostratigraphic boundary between the Cretaceous and the Palaeocene sediments at Site 1049 (Fig. 2). It sharply overlies slumped uppermost Cretaceous foraminiferal–nannofossil ooze and is overlain by Tertiary clay-rich ooze with planktonic foraminiferal assemblages indicative of Early Danian Foraminiferal Zone P-alpha (Norris *et al.* 1998, 1999). This layer mainly consists of green spherical and oval-shaped spherules mostly composed of smectite, which derives from alteration of the original material (Martínez-Ruiz *et al.* this volume) and is capped by a 3 mm-thick orange Fe-oxide layer that initially appeared to be the fireball layer (Norris, Kroon, Klaus *et al.* 1998) equivalent to the uppermost layer in non-marine sections (Pollastro & Bohor 1993). The spherule bed also contains some lithic fragments, Cretaceous foraminifera and clasts of Cretaceous material, suggesting reworking of the spherule bed material, which is further supported by the variable thickness. Notwithstanding this reworking, which limits the interpretation of the possible original stratigraphy of the ejecta deposit at Blake Nose, the ejecta fallout from the Chicxulub impact is recorded. The spherule bed was not preserved at Holes 1050C and 1052E, although at Hole 1052E some burrows are filled with ejecta material (Norris *et al.* 1998; Klaus *et al.* 2000). Samples were collected from cores 16X, 17X and 18X at Hole 1049A, taking samples continuously every 2 cm in an interval from 125.69 to 126.23 m below sea floor (mbsf) in section 17X-2 in order to analyse continuously and with higher resolution the K–T boundary layer and nearby sediments above and below. At Hole 1049B, a

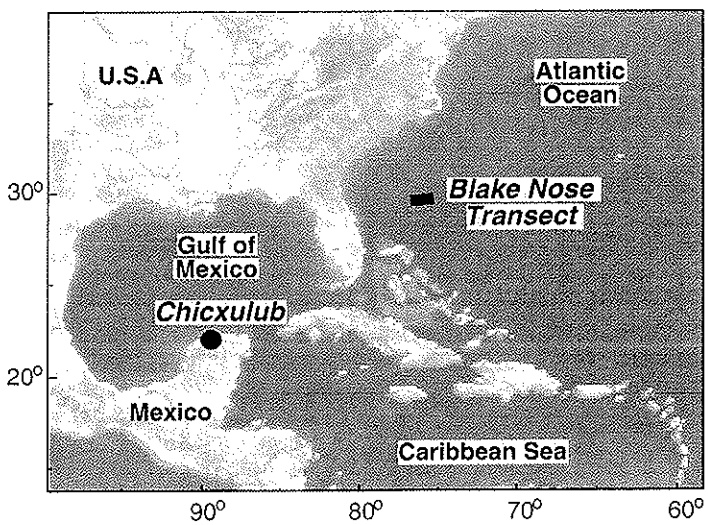

Fig. 1. Location of the ODP Leg 171B Blake Nose drilling transect.

continuous sampling of the K–T boundary interval was also carried out in section 8H-2 every 2 cm in an interval from 111.00 to 111.32 mbsf. Other scattered samples were also taken at these holes (see Tables 1 and 2 for sample position). At Holes 1050C and 1052E, where the spherule bed is not well preserved, lower-resolution sampling was carried out. Section 10R-2 was sampled at Hole 1050C, and sections 18R-1, 18R-2, 18R-3 and 19R-1 were sampled at Hole 1052E (see Tables 3 and 4 for sample positions).

Samples from the spherule bed were cleaned of Cretaceous clasts under a stereomicroscope and dried, homogenized and ground in an agate mortar for chemical analyses using inductively coupled plasma-mass spectrometry (ICP-MS) and atomic absorption spectrometry (AAS). Rb, Sr, Ba, V, Cr, Co, Ni, Cu, Zr, Hf, Mo, Pb, U, Th and rare earth elements (REE) were analysed by ICP-MS, and Al, K, Fe, Mn, Ca and Mg were analysed by AAS. Analyses were performed on bulk samples after sample digestion with HNO_3 + HF of 0.100 g of sample powder in a Teflon-lined vessel at high temperature and pressure, evaporation to dryness and subsequent dissolution in 100 ml of 4 vol. % HNO_3. ICP-MS instrument measurements were performed in

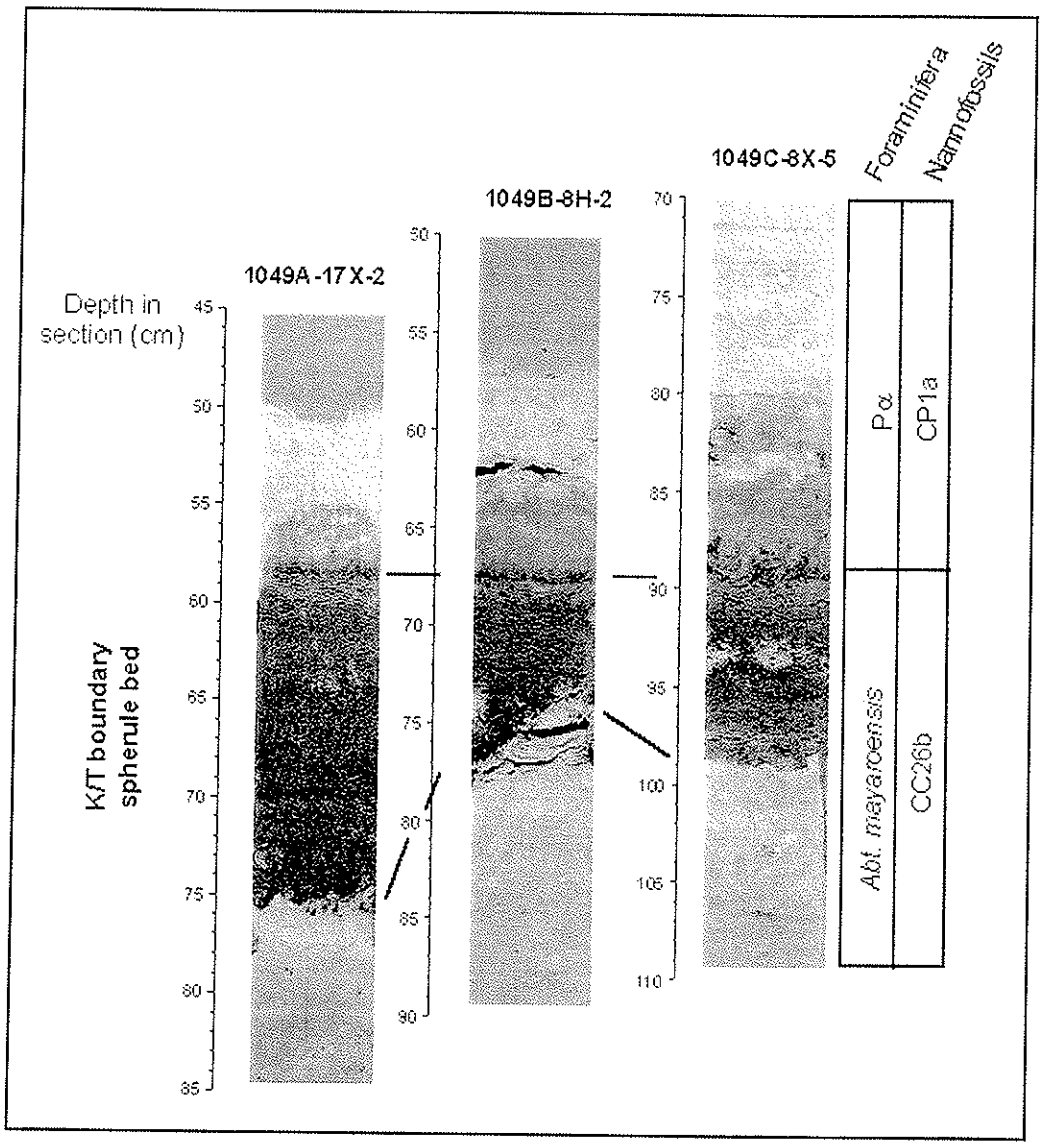

Fig. 2. Core photographs of the K–T boundary interval at Site 1049 showing the spherule bed marking the boundary at the three holes drilled at this site and its variable thickness (biostratigraphy from Norris *et al.* (1999)).

Table 1. *Geochemical data from the K–T boundary interval at Hole 1049A*

Sample	Depth (mbsf)	Al	K	Fe	Mn	Ca	Mg	Rb	Sr	Ba	V	Cr	Co	Ni	Cu	Zr	Hf	Mo	Pb	U	Th	REE	Ua
16X 01 002–004	115.02	3.14	1.09	1.40	270	21.0	0.80	46.6	607	101	64.8	134	7.97	29.0	24.2	25.6	0.60	0.29	7.37	0.47	2.75	73.33	0.52
16X 01 042–044	115.42	3.30	1.07	1.46	200	17.7	0.80	49.0	583	97	80.5	153	9.23	27.8	25.9	24.8	0.51	0.17	3.89	0.41	2.32	67.09	0.53
16X 01 093–095	115.93	3.68	1.10	1.60	590	16.5	0.92	53.2	669	101	82.3	141	8.39	29.6	20.6	25.9	0.64	0.20	4.90	0.50	3.12	74.15	0.48
16X 01 135–137	116.35	3.43	1.01	1.54	190	17.9	0.73	50.0	663	85	96.6	184	10.2	31.4	22.8	24.5	0.50	0.16	3.98	0.43	2.36	66.98	0.55
16X 02 025–025	116.75	2.80	0.89	1.29	260	20.5	0.80	39.4	637	83	48.2	93.8	6.71	21.1	12.7	20.3	0.58	0.11	4.86	0.54	2.74	76.07	0.59
16X 02 077–079	117.27	2.48	0.74	1.20	180	21.9	0.74	32.4	654	70	38.5	76.9	5.09	13.9	10.5	16.2	0.45	0.56	4.73	0.47	2.66	65.81	0.53
16X 02 122–124	117.72	2.60	0.77	1.27	230	21.8	0.74	36.8	687	73	42.7	81.1	5.52	16.3	10.5	16.3	0.50	0.28	4.96	0.43	2.78	64.61	0.46
16X 03 002–004	118.02	1.77	0.60	0.97	230	24.3	0.62	25.8	734	47	35.6	64.5	4.63	13.5	9.78	11.9	0.32	1.11	3.09	0.34	1.59	51.32	0.64
16X 03 044–046	118.44	1.55	0.50	0.80	220	14.6	0.57	24.8	788	36	41.0	66.7	4.95	13.2	9.11	10.9	0.24	0.02	2.15	0.24	1.18	44.28	0.62
16X 03 093–095	118.93	2.00	0.62	1.17	520	23.7	0.64	28.7	734	58	42.4	68.3	10.2	21.1	11.56	15.8	0.41	0.83	4.85	0.40	2.09	63.19	0.58
16X 03 132–134	119.32	1.92	0.60	1.08	320	22.7	0.62	28.8	684	59	38.8	64.3	9.55	13.7	9.59	14.7	0.40	0.79	7.18	0.39	2.05	56.53	0.57
16X 04 041–043	119.91	2.90	0.78	1.43	230	18.6	0.87	44.4	627	74	85.2	150	8.43	24.4	17.0	19.9	0.43	0.07	3.40	0.57	2.00	56.35	0.86
16X 04 099–101	120.49	3.38	0.94	1.76	280	14.1	0.99	51.3	615	104	90.4	159	7.76	23.5	20.4	23.1	0.57	0.32	4.62	0.76	2.97	73.23	0.77
16X 05 012–014	121.12	3.90	0.94	1.73	180	15.5	1.02	56.6	660	96	124	165	8.19	22.4	33.6	23.0	0.47	0.35	4.61	0.75	2.57	67.16	0.87
16X 05 069–071	121.69	2.35	0.61	1.05	230	20.4	0.70	31.1	744	73	41.5	77.2	4.31	10.6	21.5	14.7	0.39	0.36	4.36	0.76	2.29	56.88	0.99
16X 05 129–131	122.29	1.62	0.45	0.70	270	24.6	0.87	24.7	788	41	48.9	86.5	5.11	9.62	13.3	10.0	0.23	0.82	2.06	0.51	1.09	35.66	1.40
16X 06 033–035	122.83	3.13	0.85	1.42	230	17.9	0.94	48.1	564	96	94.8	113.4	11.0	22.2	10.1	22.3	0.63	0.38	5.54	1.20	3.47	82.89	1.04
16X 06 083–085	123.33	3.53	1.03	1.71	180	15.4	0.99	59.8	540	127	93.7	149	28.8	42.2	29.4	28.1	0.73	0.44	7.54	1.52	3.92	90.60	1.17
16X CC 015–017	123.82	2.82	0.89	1.38	250	19.5	0.85	46.8	557	94	69.3	117	13.1	24.8	9.44	21.0	0.55	0.20	4.92	1.38	3.37	81.44	1.22
17X 01 069–071	125.29	1.97	0.58	0.92	230	23.9	0.69	32.2	722	63	46.2	77.9	14.1	19.7	12.0	15.1	0.38	0.11	3.61	0.92	2.26	54.70	1.22
17X 02 001–003	125.32	2.05	0.61	0.56	288	31.6	0.75	39.0	764	73	39.6	75.4	12.2	24.2	<0.5	16.2	0.43	0.25	2.99	0.91	2.19	57.10	1.24
17X 02 004–006	125.35	1.89	0.54	0.52	256	31.8	0.76	35.8	763	60	36.5	66.0	10.0	20.0	<0.5	13.8	0.40	0.27	2.68	0.81	1.91	52.07	1.27
17X 02 008–010	125.39	2.46	0.76	1.03	295	30.3	0.77	42.3	722	74	44.9	75.8	13.6	26.1	2.86	16.5	0.47	0.23	3.81	0.91	2.37	61.96	1.15
17X 02 012–014	125.43	1.89	0.57	0.73	262	33.8	0.72	28.0	737	54	33.4	62.3	11.1	21.4	<0.5	12.2	0.34	0.24	3.61	0.89	1.80	49.88	1.49
17X 02 016–018	125.47	2.26	0.68	0.89	264	30.7	0.80	30.9	729	68	39.5	73.0	13.4	25.2	<0.5	14.9	0.43	0.22	3.79	1.05	2.20	57.42	1.43
17X 02 020–022	125.51	3.35	0.95	1.32	286	25.8	0.97	43.2	671	112	58.7	122	33.7	71.3	5.29	25.0	0.67	0.64	7.15	1.27	3.37	83.46	1.13
17X 02 024–026	125.55	3.48	0.91	1.34	213	23.6	0.92	55.6	663	115	67.8	117	58.1	76.1	<0.5	27.7	0.82	0.34	6.36	1.49	3.48	82.74	1.29
17X 02 028–030	125.59	2.48	0.69	0.99	249	28.8	0.75	38.2	716	79	46.9	83.0	17.2	26.5	<0.5	19.3	0.51	0.42	4.49	1.04	2.48	64.99	1.26
17X 02 032–034	125.63	2.19	0.62	0.90	247	20.7	0.72	29.2	727	69	43.5	71.0	13.6	22.2	<0.5	17.4	0.47	0.23	3.84	0.95	2.39	62.41	1.19
17X 02 035–037	125.66	2.31	0.64	0.97	271	29.6	0.75	37.4	731	71	44.5	73.6	12.8	23.8	<0.5	18.3	0.47	0.25	3.74	0.99	2.26	64.33	1.32
17X 02 038–040	125.69	2.24	0.69	0.95	304	29.9	0.75	35.8	722	69	44.2	73.4	11.0	23.1	<0.5	18.0	0.43	0.20	3.71	0.94	2.32	64.64	1.21
17X 02 040–042	125.71	2.18	0.64	0.91	300	28.6	0.71	37.5	723	70	44.1	73.2	11.0	25.5	<0.5	19.0	0.46	0.20	3.55	0.89	2.24	64.41	1.19
17X 02 042–044	125.73	2.19	0.67	0.99	305	27.5	0.74	36.1	712	70	43.7	73.0	11.0	20.6	<0.5	19.1	0.45	0.27	3.60	0.92	2.33	67.04	1.18
17X 02 044–046	125.75	2.25	0.64	0.89	285	28.4	0.75	39.9	705	73	44.3	73.4	10.0	19.2	<0.5	19.4	0.49	0.26	3.57	0.90	2.37	68.93	1.15
17X 02 046–048	125.77	2.16	0.64	1.02	298	28.0	0.72	35.7	695	70	44.0	72.2	10.3	20.7	<0.5	18.6	0.43	0.21	3.32	0.87	2.25	68.48	1.16
17X 02 048–050	125.79	2.17	0.65	1.03	291	25.4	0.68	37.5	713	71	46.4	75.8	18.5	34.5	<0.5	19.5	0.42	0.23	4.08	0.92	2.39	73.63	1.16
17X 02 050–052	125.81	1.47	0.53	0.77	350	31.2	0.61	27.0	506	48	46.3	48.6	6.88	20.1	3.50	14.7	0.36	0.17	2.44	1.04	1.68	62.72	1.86
17X 02 052–054	125.83	1.55	0.47	0.70	487	31.7	0.54	24.5	388	42	34.4	36.8	2.61	9.58	<0.5	13.9	0.38	0.13	1.81	1.11	1.65	65.39	2.01
17X 02 054–056	125.85	2.03	0.62	0.86	757	29.9	0.61	19.1	421	50	36.6	44.8	2.97	10.8	1.55	16.9	0.46	0.24	2.15	0.90	1.90	79.66	1.43
17X 02 056–058	125.87	1.80	0.61	0.91	341	29.7	0.65	30.6	424	54	36.6	44.0	3.58	14.2	2.13	19.3	0.48	0.16	4.55	0.96	2.00	86.07	1.45
17X 02 058–060	125.89	5.13	0.71	4.66	100	11.3	2.00	36.7	298	17	53.8	49.0	38.9	91.3	<0.5	103	2.46	2.34	6.33	1.03	3.38	24.85	0.92
17X 02 060–062	125.91	6.15	0.82	2.14	100	6.8	1.92	29.9	252	338	61.3	65.0	155	247	24.0	123	3.82	0.40	9.75	2.00	3.64	12.52	1.65

17X 02 062–064	125.93	6.45	0.80	2.13	100	6.1	1.88	34.5	264	198	56.1	75.7	207	293	15.2	143	4.11	0.51	11.66	2.88	4.61	14.40	1.88
17X 02 064–066	125.95	7.28	0.98	2.37	100	7.5	2.44	31.7	234	56	69.0	59.9	36.4	54.3	3.86	139	3.62	0.30	4.93	2.14	4.26	22.81	1.51
17X 02 066–068	125.97	7.64	0.79	2.12	100	4.2	2.10	30.4	142	9	74.8	61.5	26.5	39.0	6.67	144	3.83	0.32	4.24	2.41	4.80	28.60	1.51
17X 02 068–070	125.99	8.25	0.97	2.25	100	3.1	2.12	30.3	132	9	73.1	76.8	34.3	47.7	20.7	163	4.74	0.38	5.47	4.18	5.10	20.20	2.45
17X 02 070–072	126.01	8.63	1.11	1.77	100	3.4	2.00	26.4	133	43	76.0	84.3	27.3	44.9	53.0	168	4.83	0.39	5.53	4.85	4.78	24.49	3.04
17X 02 072–074	126.03	8.00	0.88	2.20	100	3.8	2.21	23.7	142	192	80.4	57.6	13.3	26.4	45.3	146	4.36	0.47	6.37	3.82	5.14	15.58	2.23
17X 02 074–076	126.05	9.25	1.04	1.86	100	5.1	1.55	64.3	167	46	68.6	92.8	91.4	86.6	89.1	165	5.10	0.60	13.16	8.18	6.03	16.01	4.07
17X 02 076–078	126.07	2.57	0.57	0.86	220	30.3	0.55	35.9	864	66	41.6	43.6	13.9	30.2	6.57	22.8	0.50	0.69	3.49	0.96	2.12	58.23	1.36
17X 02 078–080	126.09	2.54	0.62	0.87	248	29.9	0.50	37.2	880	69	36.9	44.7	38.1	71.3	13.4	19.3	0.41	0.18	3.39	0.55	2.20	63.45	0.75
17X 02 080–082	126.11	2.55	0.64	1.09	254	29.5	0.51	42.4	895	74	40.7	48.5	38.8	77.3	7.21	19.8	0.41	0.28	3.46	0.53	2.25	63.65	0.71
17X 02 082–084	126.13	2.98	0.69	1.01	288	27.2	0.53	43.8	920	92	49.9	55.8	49.7	97.9	8.27	20.5	0.46	0.26	4.33	0.54	2.64	69.76	0.62
17X 02 084–086	126.15	2.62	0.65	0.95	329	30.2	0.51	42.2	915	76	42.1	51.5	31.1	50.2	<0.5	18.6	0.39	0.22	3.05	0.52	2.45	61.54	0.64
17X 02 086–088	126.17	2.31	0.60	0.89	358	31.5	0.46	39.2	962	70	37.7	46.7	36.6	52.4	<0.5	15.0	0.33	0.20	2.70	0.46	2.16	56.75	0.65
17X 02 088–090	126.19	2.24	0.72	1.16	340	29.7	0.47	35.1	890	73	36.5	51.6	17.9	30.8	5.40	14.9	0.36	0.22	3.10	0.47	2.40	59.24	0.59
17X 02 090–092	126.21	2.08	0.73	1.05	337	29.2	0.47	25.7	881	74	35.5	42.9	34.4	44.2	5.78	14.9	0.35	0.16	4.71	0.60	2.46	59.36	0.73
17X 02 092–094	126.23	2.51	0.77	1.15	322	29.8	0.49	42.5	909	79	39.1	48.1	23.4	33.8	0.92	15.3	0.36	0.16	3.00	0.47	2.38	59.00	0.60
17X 02 096–098	126.27	2.67	0.77	1.26	326	29.9	0.52	42.6	911	85	40.5	51.1	5.31	16.9	0.83	15.8	0.38	0.15	3.36	0.46	2.54	58.81	0.54
17X 02 100–102	126.31	2.73	0.67	0.81	296	27.5	0.54	42.9	938	87	44.8	57.4	5.80	16.9	<0.5	15.7	0.39	0.21	3.39	0.46	2.80	59.48	0.50
17X 02 104–106	126.35	2.78	0.64	1.10	315	28.8	0.53	40.2	947	89	41.2	51.1	5.50	17.7	<0.5	14.0	0.37	0.24	4.32	0.45	2.59	56.52	0.52
17X 02 108–110	126.39	2.71	0.64	1.23	315	28.1	0.52	36.4	914	88	41.2	50.8	5.45	16.5	<0.5	14.8	0.40	0.26	3.15	0.44	2.70	57.02	0.48
17X 02 112–114	126.43	2.87	0.69	1.31	266	26.0	0.50	45.0	928	91	44.4	58.0	5.97	18.9	<0.5	15.2	0.39	0.27	4.28	0.44	2.74	57.53	0.48
17X 02 116–118	126.47	3.00	0.79	1.42	296	29.3	0.53	30.3	798	92	40.2	50.8	5.73	16.5	<0.5	14.4	0.43	0.25	3.96	0.49	3.04	59.29	0.49
17X 02 120–122	126.51	2.92	0.87	1.39	267	28.5	0.55	40.3	864	86	41.6	56.5	5.55	17.5	2.36	14.4	0.44	0.28	5.62	0.46	2.77	57.63	0.50
17X 02 124–126	126.55	3.05	0.89	1.45	283	27.1	0.55	48.9	870	96	43.9	57.9	5.93	21.5	1.66	15.8	0.41	0.40	6.48	0.50	3.00	58.78	0.50
17X 02 128–130	126.59	2.74	0.73	1.30	289	27.9	0.51	41.4	870	84	38.6	51.3	5.63	17.0	0.31	13.1	0.35	0.18	3.66	0.45	2.65	51.75	0.51
17X 02 132–134	126.63	2.30	0.76	1.19	314	29.8	0.46	42.3	912	77	36.1	50.0	52.5	16.8	<0.5	11.9	0.34	0.20	3.88	0.41	2.39	52.70	0.52
17X 02 136–138	126.67	2.36	0.73	1.22	293	29.0	0.46	34.1	880	77	35.6	50.3	5.36	16.0	<0.5	11.9	0.34	0.22	3.50	0.42	2.46	47.86	0.51
17X 02 148–150	126.79	2.06	0.60	1.03	260	24.3	0.31	35.1	940	68	33.8	49.8	5.12	12.1	5.95	11.0	0.31	0.05	5.05	0.47	2.06	44.49	0.68
17X 03 024–026	127.05	2.55	0.65	1.30	220	23.2	0.46	43.2	949	85	42.8	63.6	7.18	14.9	8.12	14.4	0.40	0.12	4.26	0.47	2.79	53.55	0.51
17X 03 054–056	127.35	2.22	0.66	1.17	210	32.4	0.42	42.1	951	77	38.5	61.6	7.12	13.7	7.12	12.8	0.35	0.09	370	0.45	2.51	46.98	0.53
17X 03 075–077	127.56	2.32	0.67	1.31	210	21.7	0.41	42.9	921	77	43.2	59.3	6.88	17.7	7.24	12.6	0.31	0.05	4.14	0.65	2.42	45.76	0.81
17X 03 082–084	127.63	2.27	0.66	1.24	220	23.2	0.42	41.5	937	78	44.6	66.6	7.22	15.3	5.89	12.7	0.40	0.09	3.73	0.46	2.64	47.63	0.52
17X 03 110–113	127.91	1.99	0.63	1.10	230	26.0	0.37	39.7	961	73	40.6	58.9	6.71	12.8	7.22	11.7	0.32	0.08	3.98	0.50	2.28	45.19	0.65
17X CC 026–028	128.36	2.47	0.76	1.18	260	23.5	0.46	49.5	912	84	39.6	51.3	7.87	14.3	8.89	13.8	0.39	0.06	6.20	0.60	2.59	52.77	0.69
18X 01 035–037	134.65	2.33	0.72	1.02	230	24.1	0.39	48.5	919	84	44.1	57.6	7.90	15.0	9.77	13.6	0.36	0.10	4.01	0.67	2.73	53.14	0.74
18X 01 115–117	135.45	2.39	0.73	1.11	250	26.6	0.38	49.1	914	84	42.1	57.7	7.50	15.0	10.3	13.4	0.35	0.72	4.31	0.72	25.1	50.97	0.86
18X 02 006–008	135.86	2.69	0.81	1.29	280	23.4	0.40	51.8	940	95	43.2	57.7	7.81	15.6	9.34	15.5	0.44	0.19	4.36	0.69	2.87	56.79	0.73
18X 02 057–059	136.37	2.38	0.73	1.13	240	23.4	0.39	48.0	947	82	45.2	57.3	8.04	15.2	13.2	14.1	0.39	0.07	4.38	0.83	2.71	54.21	0.92
18X 02 130–132	137.10	2.31	0.71	1.09	270	26.3	0.38	47.7	953	84	42.6	54.7	7.76	15.5	11.2	13.9	0.38	0.05	3.76	0.68	2.47	53.26	0.83
18X 03 048–050	137.78	2.43	0.76	1.18	250	24.1	0.40	52.8	956	88	47.1	58.9	8.06	15.0	11.0	15.0	0.39	0.11	3.73	0.81	2.71	54.79	0.90
18X 03 124–126	138.54	2.39	0.76	1.18	250	23.7	0.41	46.4	955	86	47.7	61.0	8.96	16.9	15.7	15.9	0.40	0.57	6.22	0.95	2.66	54.56	1.08
18X 04 011–013	138.91	2.61	0.78	1.20	220	23.9	0.39	53.1	985	89	47.9	59.4	10.6	19.1	141	16.0	0.40	0.11	8.66	22.19	2.78	53.71	23.92
18X 04 095–097	139.75	1.06	0.33	0.46	260	31.5	0.40	17.1	870	33	15.5	17.1	4.91	8.41	6.25	8.26	0.22	0.00	2.60	0.34	1.12	31.76	0.91

Ua, authigenic uranium (total U – Th/3). Al, K, Fe, Ca and Mg in wt %; others in ppm. (Shaded area corresponds to the spherule bed.)

Table 2. *Geochemical data from the K–T boundary interval at Hole 1049*

Sample	Depth (mbsf)	Al	K	Fe	Mn	Ca	Mg	Rb	Sr	Ba	V	Cr	Co	Ni	Cu	Zr	Hf	Mo	Pb	U	Th	REE	Ua
8H 01 015–017	109.15	2.44	0.67	1.03	290	22.1	0.77	35.1	717	64	82.2	100	13.4	27.2	14.8	15.9	0.38	0.18	3.47	0.74	1.90	53.07	0.11
8H 01 035–037	109.25	2.11	0.58	0.58	243	29.7	1.36	34.9	740	66	44.6	73.3	10.1	23.2	<0.5	14.9	0.41	0.40	3.20	0.81	2.03	55.62	0.13
8H 01 055–057	109.55	2.21	0.61	0.94	280	23.1	0.70	32.9	746	57	60.8	97.3	14.9	26.0	12.9	14.8	0.30	0.29	2.98	0.71	1.73	49.06	0.13
8H 01 075–077	109.75	2.30	0.63	0.97	250	23.0	0.71	31.9	713	67	41.5	66.6	12.4	17.8	11.9	14.8	0.41	0.35	4.07	0.90	2.30	58.58	0.13
8H 01 095–097	109.95	2.88	0.74	0.73	238	26.1	0.89	35.4	752	65	44.9	68.0	10.1	21.7	<0.5	15.2	0.46	0.26	3.15	0.83	2.09	54.73	0.13
8H 01 115–117	110.15	2.38	0.79	0.62	249	28.1	0.82	39.6	749	76	40.8	78.7	8.78	21.2	<0.5	17.2	0.50	0.24	3.64	0.88	2.28	57.76	0.12
8H 01 125–127	110.25	2.08	0.58	0.60	229	29.1	0.71	38.8	708	65	41.1	67.0	10.9	21.1	<0.5	14.3	0.43	0.24	2.88	0.83	2.12	56.94	0.12
8H 01 135–137	110.35	2.23	0.70	0.62	268	30.0	0.77	35.0	698	69	41.6	69.3	16.8	31.1	3.65	15.6	0.46	0.22	3.40	0.89	2.27	58.67	0.12
8H 01 145–147	110.45	2.16	0.69	0.62	263	30.2	0.75	25.9	697	69	41.9	68.1	12.7	27.2	1.67	14.8	0.42	0.27	3.88	1.00	2.35	61.26	0.21
8H 02 003–005	110.53	2.07	0.69	0.65	266	30.2	0.73	35.9	718	68	42.8	71.9	12.3	24.5	<0.5	15.9	0.41	0.26	3.56	0.90	2.16	59.36	0.18
8H 02 010–012	110.60	2.18	0.77	0.64	272	29.7	0.72	34.3	700	70	42.1	70.8	12.7	25.0	<0.5	15.6	0.45	0.24	3.80	0.94	2.29	61.47	0.17
8H 02 016–018	110.66	2.33	0.73	0.70	297	30.9	0.76	34.8	707	69	42.7	70.6	13.5	25.8	2.56	15.8	0.43	0.33	3.56	0.97	2.34	62.04	0.19
8H 02 023–025	110.73	2.21	0.75	0.67	264	32.4	0.75	36.5	721	69	43.8	72.4	13.1	24.1	<0.5	16.7	0.50	0.33	3.48	0.89	2.30	63.03	0.12
8H 02 031–033	110.81	2.17	0.75	0.63	262	21.0	0.77	33.4	677	68	41.4	68.1	23.8	35.9	<0.5	16.4	0.47	0.25	3.94	0.90	2.33	64.66	0.12
8H 02 038–040	110.88	2.71	0.70	0.65	244	28.7	0.78	41.6	711	82	51.8	83.2	12.7	24.4	<0.5	20.7	0.56	0.29	4.32	1.03	2.68	73.20	0.14
8H 02 045–047	110.95	2.41	0.65	0.60	231	29.4	0.78	37.2	706	72	44.7	73.7	11.3	28.5	<0.5	19.1	0.47	0.19	3.61	0.92	2.35	69.81	0.13
8H 02 050–052	111.00	2.42	0.64	1.07	254	29.6	0.72	41.7	710	74	46.4	76.6	14.1	27.1	<0.5	20.3	0.44	0.24	3.48	0.90	2.34	74.41	0.12
8H 02 052–054	111.02	2.40	0.63	1.05	273	30.4	0.70	38.3	722	75	45.4	76.8	16.5	32.6	<0.5	22.3	0.53	0.39	3.83	0.88	2.33	75.90	0.10
8H 02 054–056	111.04	2.29	0.65	0.95	255	29.7	0.69	30.6	693	71	52.1	72.4	22.0	44.6	<0.5	20.8	0.50	0.22	4.27	0.90	2.30	75.30	0.13
8H 02 056–058	111.06	1.97	0.54	0.87	315	31.2	0.61	30.7	526	57	52.7	55.4	11.8	20.6	7.69	17.7	0.44	0.24	2.76	0.88	1.98	77.39	0.22
8H 02 058–060	111.08	1.50	0.43	0.71	295	32.6	0.57	19.1	403	42	31.7	38.0	3.5	10.9	<0.5	15.6	0.40	0.23	1.53	1.05	1.63	73.18	0.50
8H 02 060–062	111.10	2.03	0.51	0.91	239	30.9	0.72	23.4	454	51	36.2	44.4	3.8	13.0	<0.5	19.8	0.48	0.15	2.05	0.95	1.92	79.76	0.31
8H 02 062–064	111.12	3.52	0.75	1.59	206	22.7	1.53	43.8	442	60	52.8	52.8	12.1	46.6	14.8	43.2	1.06	0.32	3.35	1.08	3.11	77.67	0.05
8H 02 064–066	111.14	3.83	0.75	0.99	197	18.8	1.65	39.4	418	54	55.6	46.5	22.3	93.7	18.8	47.3	1.27	0.34	4.07	0.99	4.17	71.49	−0.40
8H 02 066–068	111.16	3.61	0.57	4.91	50	7.8	1.94	20.0	258	13	64.1	47.1	75.4	115	16.7	67.2	1.42	3.51	8.62	0.75	2.94	11.76	−0.23
8H 02 068–070	111.18	7.33	0.69	1.13	<50	7.6	1.85	37.8	277	293	58.1	95.7	287	433	19.9	130	3.87	0.63	9.43	2.18	4.36	9.36	0.72
8H 02 070–072	111.20	7.48	0.66	1.96	<50	7.3	1.82	37.8	288	135	65.4	76.2	160	225	24.3	118	2.30	0.40	7.70	2.29	6.07	12.77	0.26
8H 02 072–074	111.22	6.89	0.77	2.07	<50	8.1	1.72	36.4	311	322	63.1	122	277	295	58.9	134	3.76	0.59	12.15	3.40	4.13	10.26	2.02
8H 02 074–076	111.24	6.34	0.91	2.63	<50	8.2	1.78	44.6	312	15	89.6	88.7	44.6	60.9	53.6	125	3.73	0.47	7.33	2.26	3.29	13.86	1.16
8H 02 076–078	111.26	2.25	0.54	0.96	199	31.3	0.47	34.5	895	62	31.7	42.1	12.5	23.4	<0.5	18.2	0.36	0.17	2.97	0.50	2.21	56.57	−0.24
8H 02 078–080	111.28	1.97	0.61	0.90	229	33.8	0.42	30.4	907	66	33.8	41.1	8.9	21.5	<0.5	18.2	0.36	0.17	3.56	0.38	1.98	55.18	−0.28
8H 02 080–082	111.30	2.17	0.65	1.10	218	31.0	0.42	43.1	917	71	35.1	44.8	11.0	20.8	<0.5	18.9	0.41	0.17	2.65	0.40	2.15	59.28	−0.32
8H 02 082–084	111.32	2.11	0.74	1.07	226	32.5	0.39	46.4	924	69	34.1	43.6	15.6	24.6	<0.5	17.8	0.39	0.16	2.69	0.42	2.16	58.32	−0.30

Ua, authigenic uranium (total U – Th/3). Al, K, Fe, Ca and Mg in wt %; others in ppm. (Shaded area corresponds to the spherule bed.)

Table 3. *Geochemical data from the K–T boundary interval at Hole 1050C*

Sample	Depth (mbsf)	Al	K	Fe	Mn	Ca	Mg	Rb	Sr	Ba	V	Cr	Co	Ni	Cu	Zr	Hf	Mo	Pb	U	Th	REE	Ua
10R 02 010–012	405.70	1.96	0.49	1.02	340	25.4	0.62	25.1	548	56	42.0	57.4	6.11	12.6	18.0	13.7	0.42	0.22	8.95	1.12	2.29	56.70	0.35
10R 02 025–027	405.85	2.18	0.55	1.34	440	23.2	0.62	31.0	510	65	40.2	57.6	6.15	15.3	8.27	18.1	0.56	0.24	4.56	0.77	2.73	69.44	−0.14
10R 02 033–035	405.93	1.90	0.47	1.15	160	24.8	0.58	29.0	518	53	31.6	43.6	5.01	13.8	6.59	14.9	0.49	0.24	3.75	0.59	2.43	63.34	−0.22
10R 02 040–042	406.00	1.76	0.45	1.99	350	27.9	0.37	25.9	956	66	34.5	56.2	4.76	10.6	5.06	13.6	0.40	0.09	2.75	0.49	2.03	50.52	−0.19
10R 02 044–046	406.04	2.71	0.58	1.47	160	21.1	0.47	38.4	920	86	45.5	73.4	8.02	19.4	7.63	17.4	0.47	0.14	6.45	0.56	3.19	57.42	−0.51
10R 02 048–050	406.08	3.25	0.61	1.55	100	20.2	0.56	40.0	957	97	39.4	64.7	8.23	24.7	8.26	17.3	049	0.23	5.42	0.52	3.43	58.22	−0.62
10R 02 055–057	406.15	2.28	0.56	1.20	440	23.2	0.44	35.2	988	90	36.3	59.8	5.58	15.1	12.4	15.9	0.46	0.21	7.74	0.56	2.82	60.88	−0.37
10R 02 060–062	406.20	2.32	0.59	1.38	340	22.4	0.45	36.9	1004	96	39.5	63.6	6.41	16.3	26.3	17.1	0.49	0.32	6.12	0.60	2.98	61.45	−0.39
10R 02 068–070	406.28	2.81	0.61	1.48	120	21.2	0.54	38.0	989	96	41.7	70.8	7.42	18.8	27.8	16.4	0.47	0.28	5.14	0.62	3.06	60.55	−0.40
10R 02 078–080	406.38	2.31	0.56	1.31	120	22.7	0.45	33.7	1005	96	40.2	65.0	7.48	18.6	24.2	15.5	0.46	0.93	5.92	0.65	2.95	57.79	−0.33

Ua, authigenic uranium (total U – Th/3). Al, K, Fe, Ca and Mg in wt %; others in ppm.

Table 4. *Geochemical data from the K–T boundary interval at Hole 1052E*

Sample	Depth (mbsf)	Al	K	Fe	Mn	Ca	Mg	Rb	Sr	Ba	V	Cr	Co	Ni	Cu	Zr	Hf	Mo	Pb	U	Th	REE	Ua
18R 01 065–068	300.75	2.30	0.59	1.10	120	22.5	0.84	31.0	1003	89	38.9	78.5	5.68	13.1	11.3	16.3	0.48	0.17	4.55	1.00	2.59	57.91	0.13
18R 01 105–108	301.15	1.84	0.51	0.93	160	23.4	0.87	27.4	940	70	36.4	69.9	4.00	11.0	6.17	13.7	0.41	0.11	3.78	1.01	2.45	50.16	0.19
18R 01 145–148	301.55	1.88	0.51	0.98	130	24.9	0.85	28.1	949	69	36.1	66.1	5.54	15.1	10.8	14.2	0.40	0.17	4.43	1.12	2.32	48.51	0.34
18R 02 013–017	301.73	1.81	0.48	0.88	240	25.4	0.78	25.5	938	61	35.3	64.2	5.09	13.0	12.4	14.4	0.40	0.16	4.06	1.08	2.12	50.62	0.37
18R 02 029–032	301.89	1.94	0.52	0.93	340	24.5	0.82	27.5	935	66	35.2	66.5	5.12	14.5	7.76	15.4	0.42	0.15	3.79	1.25	2.19	55.36	0.51
18R 02 043–046	302.03	2.29	0.58	1.05	480	22.0	0.89	32.7	894	81	42.3	78.6	6.70	19.0	12.2	19.3	0.54	0.16	4.72	1.36	2.78	65.67	0.43
18R 02 048–051	302.08	2.61	0.65	1.20	460	20.5	0.88	36.7	907	91	43.9	81.0	10.1	24.9	8.06	22.9	0.61	0.17	5.04	1.50	2.98	72.07	0.50
18R 02 051–054	302.11	1.66	0.43	0.94	70	25.3	0.86	21.2	584	46	32.1	41.5	7.10	18.5	8.28	17.0	0.47	0.21	4.09	1.06	2.05	56.40	0.38
18R 02 057–059	302.16	1.16	0.32	0.71	100	25.6	0.88	14.3	518	28	19.9	25.6	3.93	11.1	4.97	12.1	0.34	0.11	3.63	0.82	1.36	39.29	0.37
18R 03 000–004	302.21	2.27	0.53	1.16	80	22.3	0.59	32.3	1079	79	35.5	53.3	3.57	8.19	16.8	16.3	0.55	0.11	4.20	0.60	2.78	55.65	−0.32
18R 03 027–030	302.48	2.12	0.49	1.10	150	22.2	0.62	30.3	1074	78	34.8	51.7	4.27	10.5	9.81	14.2	0.39	0.10	5.40	0.52	2.70	53.04	−0.38
18R 03 052–055	302.73	2.31	0.54	1.24	120	24.8	0.65	31.6	1060	99	36.7	54.9	4.46	10.0	6.34	14.9	0.41	0.08	4.71	0.52	2.96	56.37	−0.46
19R 01 024–027	309.94	2.65	0.64	1.28	160	22.8	0.56	46.1	1146	117	42.5	66.0	7.29	15.8	11.1	14.6	0.44	0.23	6.19	0.99	3.39	59.39	−0.14
19R 01 053–056	310.23	2.69	0.65	1.23	130	21.6	0.52	43.0	1143	121	43.0	63.0	5.96	12.7	12.0	14.5	0.48	0.24	5.99	1.02	3.28	56.33	−0.07
19R 01 099–102	310.69	2.34	0.61	1.21	1.60	21.4	0.51	41.6	1099	112	40.0	60.7	6.98	15.4	10.3	14.6	0.46	0.19	5.41	0.93	3.23	53.81	−0.14

Ua, authigenic uranium (total U – Th/3). Al, K, Fe, Ca and Mg in wt %; others in ppm.

triplicate using a Perkin Elmer Sciex Elan-5000 spectrometer with Rh as internal standard, and AAS analyses were carried out with a Perkin Elmer 5100 ZL spectrometer. The quality of the analyses was monitored with laboratory and international standards from the United States Geological Survey (USGS). ICP-MS precision and accuracy were better than ±2% and ±5% relative for analyte concentrations of 50 and 5 ppm in the rock, respectively. AAS analytical error was <2%.

Ir analyses of bulk samples were carried out by neutron activation at Centre des Faibles Radioactivés, Gif-sur-Yvette. Iridium was counted with a γ–γ spectrometer detecting the 316–468 keV γ-ray coincidence resulting from the decay of ^{192}Ir (Rocchia *et al.* 1990).

Element stratigraphy across the K–T boundary

The chemical data from analyses performed on all selected samples from the K–T boundary interval at Blake Nose are presented in Tables 1–4, corresponding to Holes 1049A, 1049B, 1050C and 1052E, respectively, and are plotted in Figs 3–7. Figure 3 represents the entire analysed interval at Hole 1049A, although the closely spaced samples at the K–T boundary bed and nearby sediments above and below are not clearly visible in this graph. Therefore, a selected interval showing the K–T boundary chemical composition in greater detail has been plotted in Fig. 4. When analysing sediments with considerable variations in carbonate content, as is the case for K–T boundary interval sediments, some fluctuations in elemental contents may result from variations in the carbonate/aluminosilicate ratio. Whole-rock concentrations of elements have, therefore, been normalized to Al as an index of the relative abundance of detrital phases and plotted in Figs 3–7. Figures 8 and 9 show the Ir profiles at the K–T boundary interval in Holes 1049A and 1049B.

Al and Ca are plotted in Figs 3–7 to give an idea of the abundances of detrital and biogenic material. As occurs in other K–T sections, the boundary is marked by a significant decrease in carbonate content as a consequence of the mass extinction and deposition of the impact fallout material. Figure 4 shows these Al and Ca variations and also the element abundance variations across the K–T boundary at Hole 1049A. As the boundary layer is better preserved at this hole, our discussion will focus on this interval and the geochemical record will then be compared with the interval analysed in the other holes.

Sr and Mg

Because Sr is closely related to Ca and carbonates, the Sr and Ca contents across the K–T boundary show a similar decrease in concentration (Tables 1 and 2), and, therefore, the Sr/Ca ratio has been considered and plotted in Figs 3–7. Even considering whole-rock analysis data, the observed decrease in Sr content in relation to Ca content across the boundary suggests a response to a global Sr decrease in early Tertiary time, reported also at other K–T boundary sections (Renard 1986). When whole-rock Mg data are considered, the profile would be expected to show a significant increase in the Mg content of the spherule bed (Tables 1 and 2) as a consequence of the decrease in carbonates and an increase in smectites. However, the Mg content normalized to Al shows an increase in Mg across the boundary which is also consistent with a global trend (Renard 1986). Variations in the Sr and Mg contents are also in good agreement with data from Hole 1049C (Speed & Kroon 2000). Although further analyses on the carbonate fraction are needed, these variations in Mg and Sr concentration seem to correlate with sea-level changes and global fluctuations.

Redox-sensitive elements and diagenetic remobilization

In the analysed interval, the Fe and Mn profiles are mainly governed by diagenetic remobilization. At Hole 1049A, where a thicker interval has been analysed, the Fe concentration is similar in Cretaceous and in Tertiary sediments (Fig. 3), suggesting similar detrital fluxes and palaeoceanographic conditions. However, the K–T boundary is marked by a significant Fe increase in the top part of the boundary bed (Fig. 4) and lower Fe and Mn concentrations within the boundary bed; the enhanced concentrations of these elements indicate diagenetic remobilization. After the mass extinction, oxygen consumption would have been enhanced by oxidation of the accumulated organic matter, and suboxic or reducing conditions would be expected after deposition. In such conditions, elements sensitive to changes in redox conditions, such as Fe and Mn, would have undergone severe redistribution. These oxygen-depleted conditions led to diffusion of Fe and Mn, precipitated upon encountering oxygenated pore waters, being oxidized and immobilized as oxyhydroxides. The two elements became decoupled during diagenesis, the Mn peak being located above the Fe peak (Fig. 4), which constrains the Eh conditions at which Fe was immobilized and Mn continued to diffuse upward upon encountering more oxygenated pore waters. Such Fe diagenetic remobilization

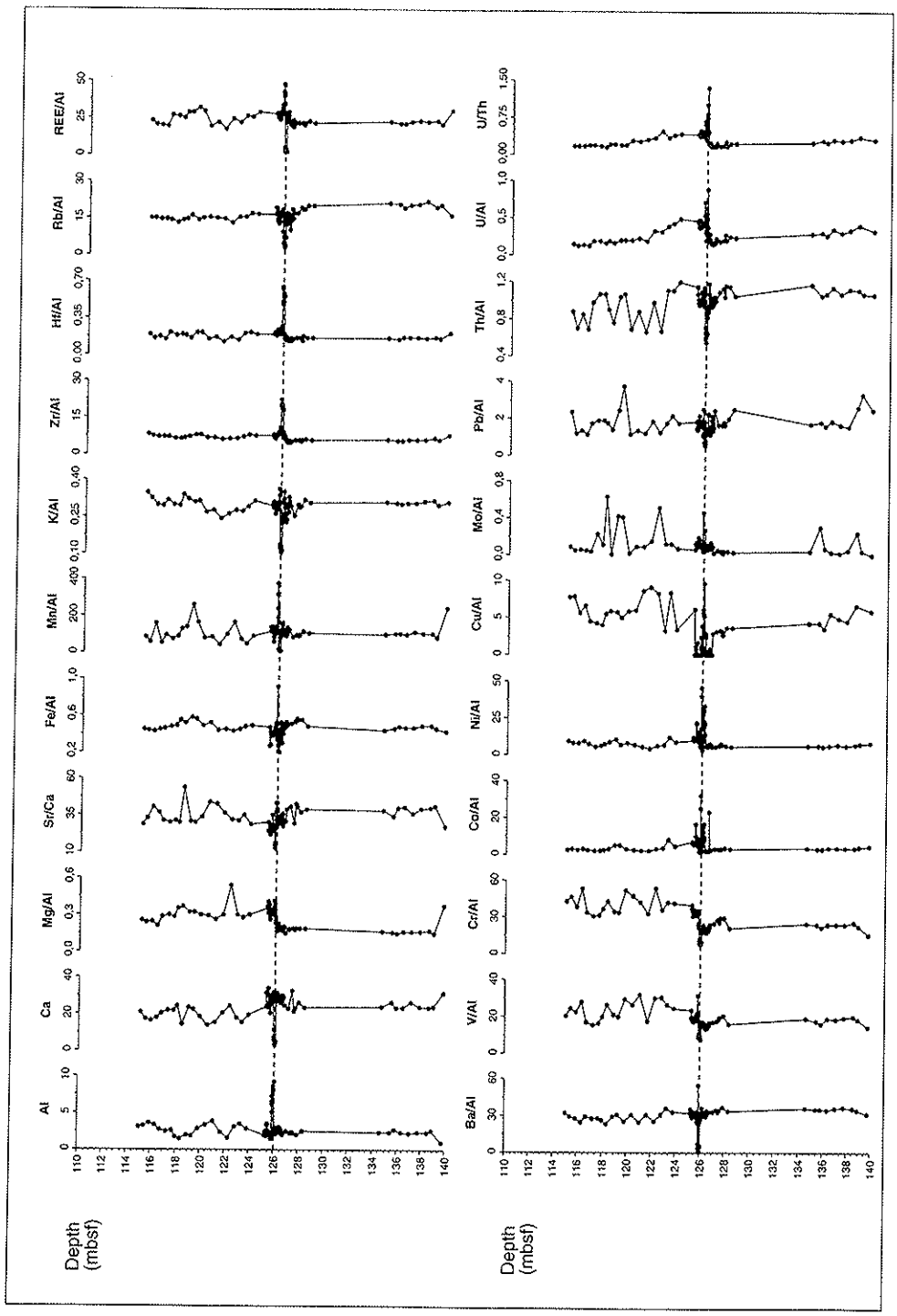

Fig. 3. Geochemical data from the K–T boundary interval at Hole 1049A. Plots show the Ca and Al concentrations (wt %), Sr/Ca and Th/U ratios, Fe, K and Mg concentrations normalized to Al and trace-element/Al weight ratio ($\times 10^4$) v. depth profiles.

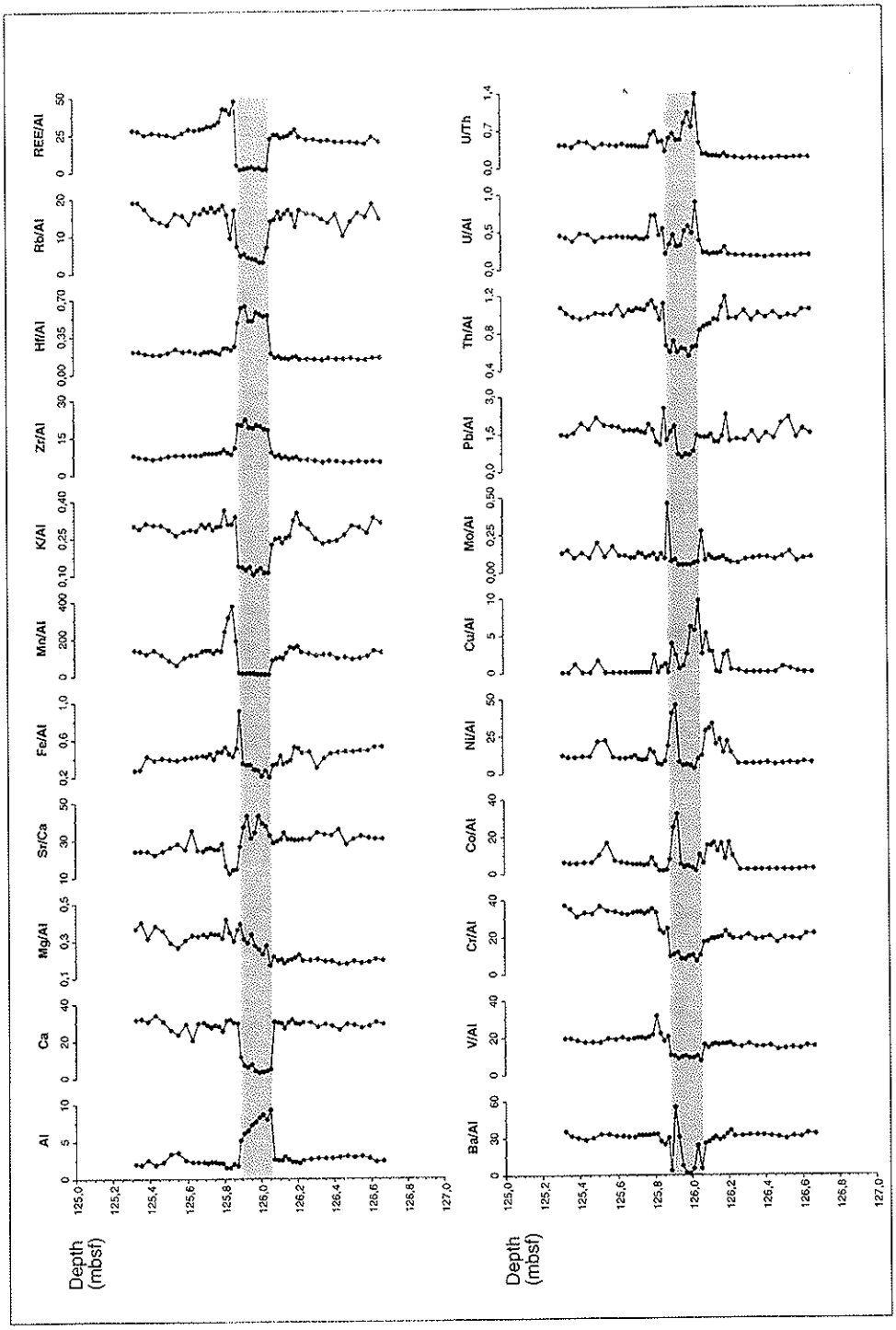

Fig. 4. Enlarged detail of K–T boundary interval showed in Fig. 3 presenting the K–T chemical profiles of the spherule bed and adjacent sediments at Hole 1049A. (Shaded area represents the spherule bed.)

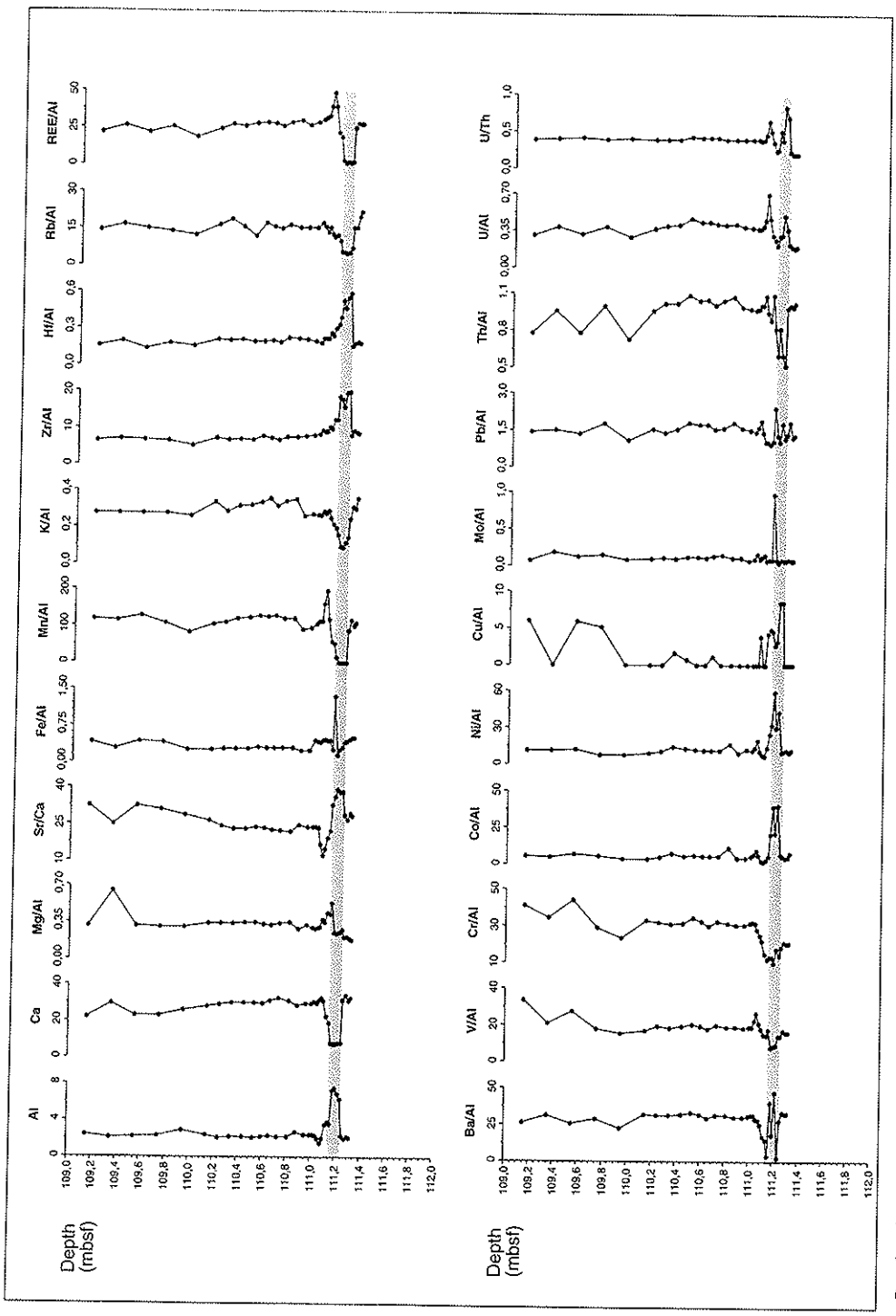

Fig. 5. Geochemical data from the K–T boundary interval at Hole 1049B. Plots show the Ca and Al concentrations (wt %), Sr/Ca and Th/U ratios, Fe, K and Mg concentrations normalized to Al and trace-element/Al weight ratio ($\times 10^4$) v. depth profiles. (Shaded area represents the spherule bed.)

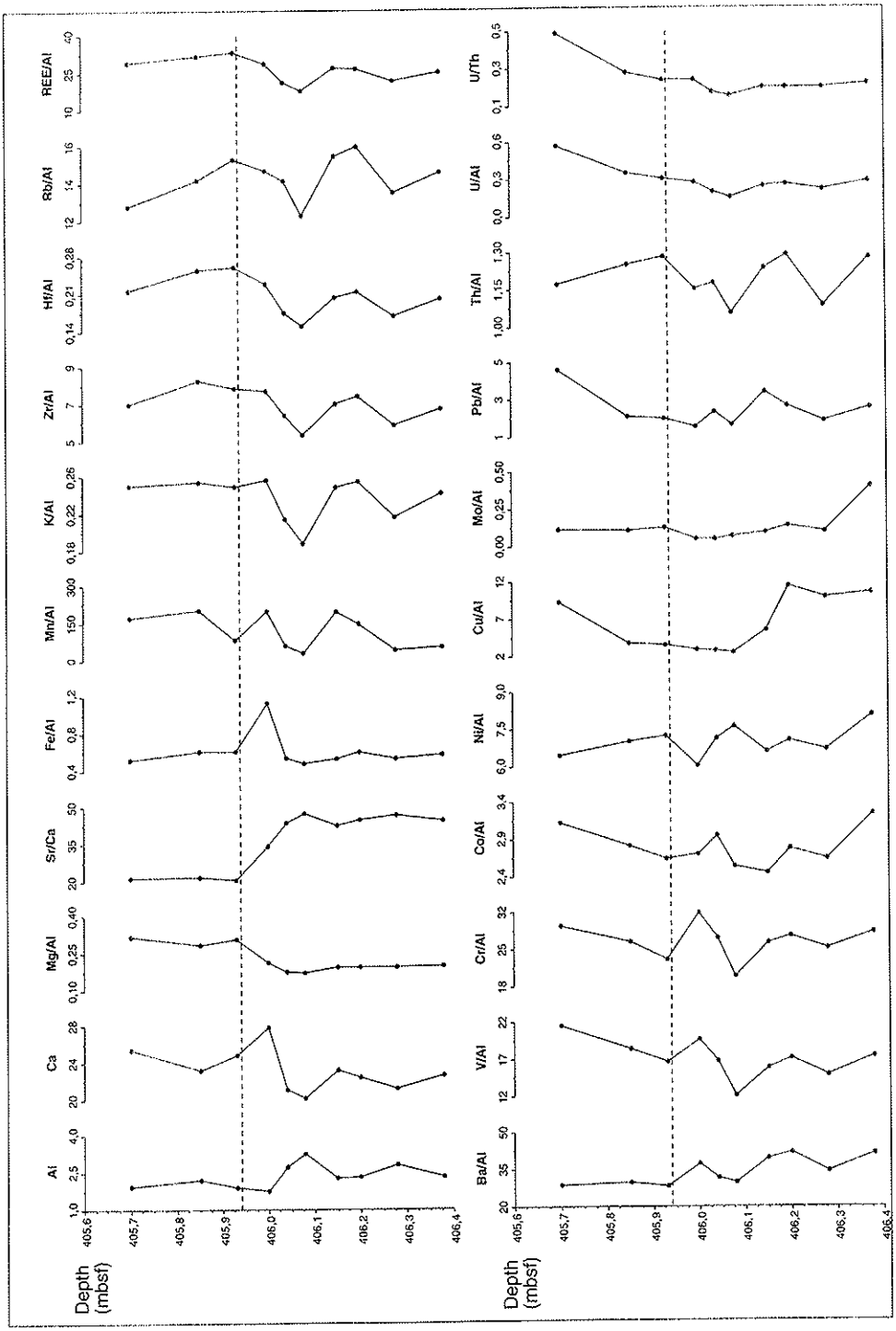

Fig. 6. Geochemical data from the K–T boundary interval at Hole 1050C. Plots show the Ca and Al concentrations (wt %), Sr/Ca and Th/U ratios, Fe, K and Mg concentrations normalized to Al and trace-element/Al weight ratio ($\times 10^4$) v. depth profiles. (The dashed line marks the K–T boundary.)

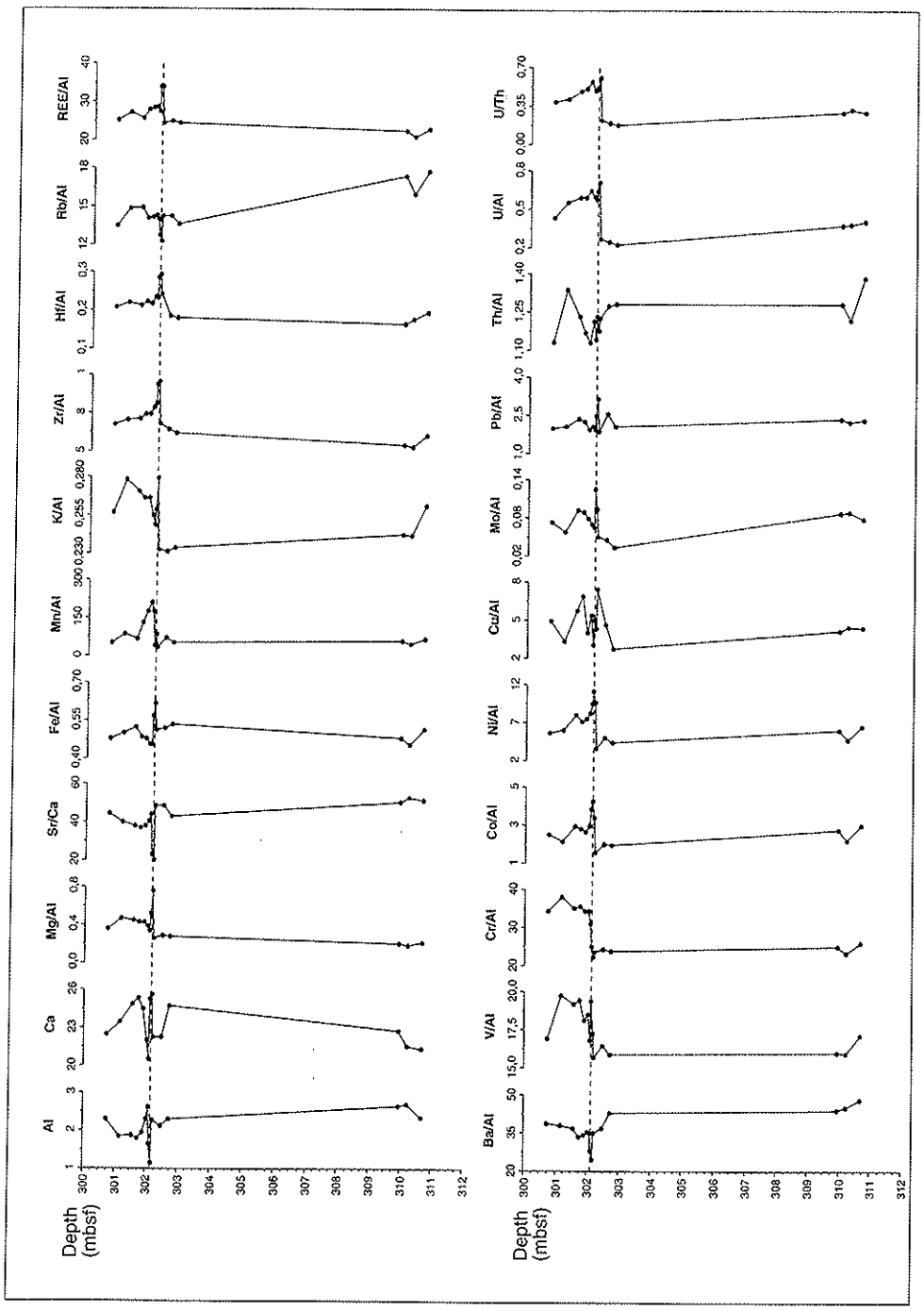

Fig. 7. Geochemical data from the K–T boundary interval at Hole 1052E. Plots show the Ca and Al concentrations (wt %), Sr/Ca and Th/U ratios, Fe, K and Mg concentrations normalized to Al and trace-element/Al weight ratio ($\times 10^4$) v. depth profiles. (The dashed line marks the K–T boundary.)

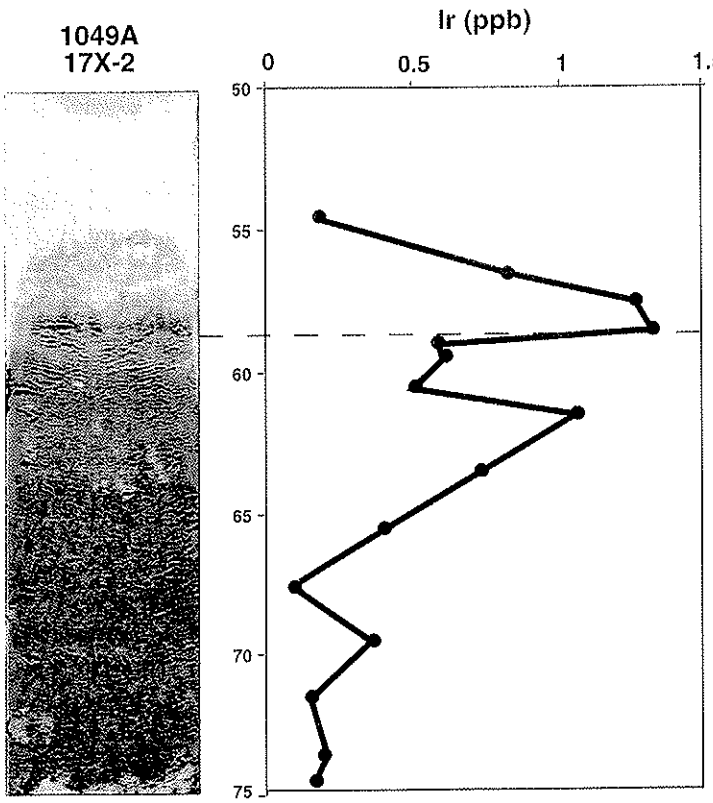

Depth (cm in core)	Ir (ppb)
54.0	0.20 ± 0.05
56.0	0.82 ± 0.10
57.0	1.26 ± 0.10
58.0	1.32 ± 0.12
58.5	0.60 ± 0.08
59.0	0.62 ± 0.10
60.0	0.50 ± 0.08
61.0	1.05 ± 0.12
63.0	0.71 ± 0.10
65.0	0.38 ± 0.10
69.0	0.28 ± 0.10
71.0	0.12 ± 0.10
73.0	0.20 ± 0.10
74.0	0.18 ± 0.10

Fig. 8. Profile of Ir content at Hole 1049A (sample at 58.5 cm depth in core corresponds to the orange Fe-oxide layer).

is responsible for the 3 mm thick rusty layer capping the spherule bed (Fig. 2) that initially appeared to be the fireball layer (Norris *et al.* 1998), but only represents in fact a diagenetic concentration of Fe, with no enhanced extra-terrestrial-element flux observed, as discussed below. At Hole 1049B where the spherule bed is preserved, and Hole 1052E, with burrows containing spherules, the same Fe and Mn patterns are observed.

Reducing conditions are also constrained by the U/Th ratio, which is a potential palaeoredox indicator. Th is relatively immobile in the sedimentary environment and is concentrated in the detrital fraction associated with heavy minerals or clays. In contrast, the U concentration is dependent on redox conditions. U^{6+} is soluble, but U^{4+} is precipitated, therefore, concentrating in a reducing environment and raising the U/Th ratio. Wignall & Myers (1988) proposed the authigenic U content (Ua) as an index of bottom-water oxygenation calculated as (authigenic U) (total U) – Th/3, which can be a reliable redox proxy (Jones & Manning 1994). The U/Th ratio and Ua content (Figs 4 and 5; Tables 1–3) reach higher values in the spherule bed, indicating more reducing conditions.

Ba also shows some fluctuations in its content in the spherule bed, governed by diagenetic remobilization. In deep-sea sediments, bulk Ba is associated with the detrital fraction, with carbonates, or it occurs as authigenic or biogenic barite. It is known that Ba has enhanced concentrations in pelagic sediments that are deposited in high-productivity areas, as it has a strong biogenic association, and its content increases with higher biogenic production (Goldberg & Arrhenius 1958; Schmitz, 1987; Dymond *et al.* 1992; Paytan *et al.* 1993; Paytan 1995). The Ba/Al ratio gives a general idea of the Ba associated with carbonates or biogenic barite, and although any palaeoproductivity interpretation would require an evaluation of biogenic barite concentration (e.g. Paytan *et al.* 1993; Paytan 1995), the slight decreases in Ba above the spherule bed could be related to lower

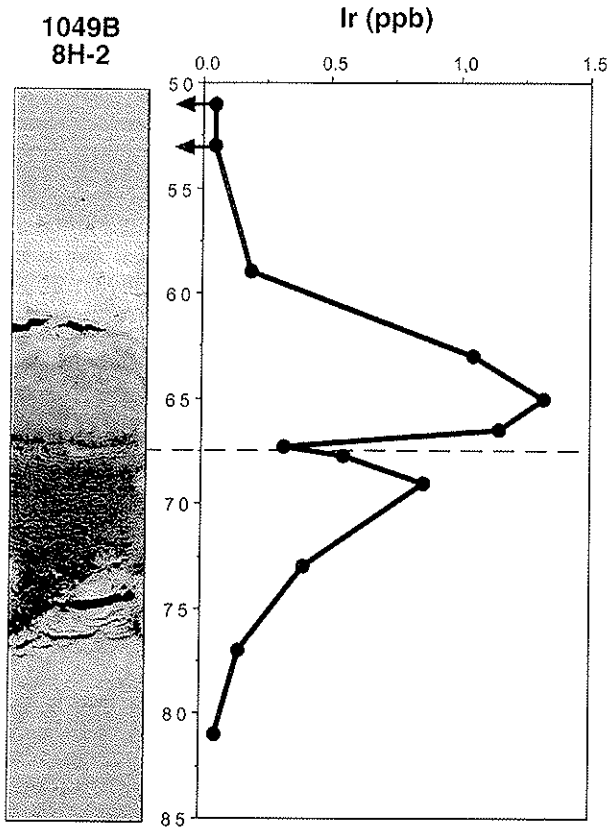

Depth (cm in core)	Ir (ppb)
51.00	≤ 0.05
53.00	≤ 0.05
59.00	0.19 ± 0.03
63.00	1.05 ± 0.07
65.00	1.32 ± 0.06
66.50	1.15 ± 0.08
67.25	0.32 ± 0.03
67.75	0.55 ± 0.09
69.00	0.86 ± 0.08
73.00	0.40 ± 0.07
77.00	0.15 ± 0.03
81.00	0.06 ± 0.03

Fig. 9. Profile of Ir content at Hole 1049B (sample at 67.25 cm depth in core corresponds to the orange Fe-oxide layer).

productivity. The low carbonate content and the absence of biogenic barite in the spherule bed led to low Ba contents (Tables 1 and 2). Ba in this bed is probably associated with the aluminosilicate fraction and secondary barite, as the enhanced Ba content within the upper part of the spherule bed also suggests diagenetic remobilization of Ba during suboxic diagenesis.

The V, Mo and Cu profiles are significantly affected by changes in redox conditions and diagenetic remobilization as well. The V content increases above the spherule bed, similar to Mn, and it may have been mobilized upward and precipitated with oxidized phases. A similar profile for Mo with an enrichment at the top of the spherule bed also indicates redistribution of this element.

Detrital elements

Detrital element profiles are governed by source material and mineral composition. The decrease in K content is related to changes in the composition of the clay mineral assemblages and the absence of illite in the spherule layer. In the Cretaceous and Tertiary sediments, clay mineral associations are composed of smectite, illite, kaolinite and minor proportions of chlorite (Martínez-Ruiz *et al.* 2000), whereas the spherule bed is mainly composed of smectite (Martínez-Ruiz *et al.* this volume) of authigenic origin. Typical detrital elements associated with detrital clays have lower concentrations in this bed. In addition, diagenetic alteration of the ejecta material led to REE depletion (Tables 1 and 2). These circumstances would explain the decrease in K, Rb, REE, Pb and Th. In fact, severe changes in major and trace element composition may have occurred during the alteration of the ejecta material to smectite. Izett (1991) examined Haitian spherules, and showed that some trace elements are severely depleted in smectite relative to the impactite glass (Izett 1991, Table 5). Thus, Cr or Rb could have been severely depleted. Izett's analyses also showed depletion in Zr and Hf, although both these elements are abundant

in the spherule bed at Blake Nose, probably derived from rutile and zircon, which have been reported by scanning electron microscopy analyses.

Extraterrestrial elements

Because diagenetic alteration limits the interpretation of extraterrestrial Fe, other typical extraterrestrial elements are considered to evaluate the possible extraterrestrial contribution in Blake Nose sediments. The Ir concentration is very low at Blake Nose (Smit *et al.* 1997), reaching the highest concentration above the spherule bed in the burrow-mottled calcareous ooze (Figs 8 & 9). The contents of Cr, Co and Ni present different profiles at this location. The Cr content decreases considerably in the spherule bed, which points to the absence of a significant extraterrestrial Cr contribution. Although Co and Ni concentrations are not as high as in distal sections, both elements are enriched in the upper part of the spherule bed, suggesting a possible enrichment derived from extraterrestrial material. Although the main contribution to the Blake Nose spherule bed is target rock material from Chicxulub it seems to have been associated with the finest fraction and therefore deposited after the spherule bed material, although diagenetic remobilization during suboxic diagenesis could also have been an important factor in Ir distribution at this location. Ir reaches its maximum content just above the orange Fe-oxide layer (Figs 8 & 9).

Comparison with other K–T ejecta deposits

The Chicxulub impact resulted in ejecta deposits identified in outcrops and drill cores world-wide (e.g. Alvarez *et al.* 1995; Pierazzo & Melosh 1999; Smit 1999), with melted target rocks deposited closer to the crater site. A major terrestrial contribution is, therefore, expected at Blake Nose. The vertically-expanding hot vapour plume of vaporized bolide with some entrained melted target rocks was dispersed and deposited globally (the fireball layer). In some K–T boundary sections, such as North American nonmarine sections, a dual nature of the K–T boundary interval is clearly evident (e.g. Pollastro & Bohor 1993), and in distal marine sections, such as those in SE Spain, only a single clay layer, equivalent to the uppermost layer in nonmarine sections, records the boundary event. In the basinal Gulf of Mexico and the Caribbean, the K–T boundary is marked by a mixture of reworked microfossils, impact-derived material and lithic fragments deposited by giant gravity flows, the K–T boundary 'cocktail' (Bralower *et al.* 1998). Impact signatures and geochemical anomalies are, therefore, different in proximal and distal locations, also as a function of different diagenetic environment. At Blake Nose, the major contribution of ejecta material is derived from target rocks, and the geochemical composition of the spherule bed reflects the composition of the precursor material modified by diagenetic alteration and presents minor extraterrestrial contribution. At distal locations, the nature of the spherules, which are microkrystites (Smit *et al.* 1992), and other impact signatures such as Ni-rich spinels (Bohor *et al.* 1986), indicate a different nature of the impact-derived material. Broadly speaking, after an impact the projectile material is ejected first and attains the highest speed, whereas the target material is ejected later and is slower (e.g. Melosh & Vickery 1991). The deposition of the impact-melted target rocks from Chicxulub, mainly consisting of impact glasses (e.g. Koeberl & Sigurdsson 1992), would have occurred quickly after the impact and more rapidly than deposition of the finest fraction derived from a cloud of vaporized bolide and entrained target-rock material. This material, usually termed the fireball layer, was deposited by gravitational processes on top of the recently deposited target-rock-derived material (e.g. Pollastro & Bohor 1993). Reworking of the K–T boundary material at Blake Nose (Klaus *et al.* 2000) prevented the preservation of the ejecta layer stratigraphy, although enhanced concentrations of Ir, Co and Ni in the upper part of the spherule bed suggest a more significant extraterrestrial contamination within this part. Nevertheless, no clear evidence for significant contribution of extraterrestrial material is observed at Blake Nose. The nature of the spherules and geochemical composition of the spherule bed suggest it is composed mostly of target-rock material, with very low amounts of bolide-derived material.

Conclusions

The K–T boundary at Blake Nose is marked by a spherule bed up to 17 cm thick at ODP Site 1049 containing green spherules, composed mostly of smectite. Reworking of the spherule material limits the interpretation of the possible original stratigraphy, but this layer none the less provides further evidence for the deposition of the Chicxulub impact-generated material, and it represents the impact-melted target rocks. Ir and other extraterrestrial elements show lower concentrations than at distal locations. Only Ni

and Co have higher concentrations within the upper part of the spherule bed. Original concentrations have been severely modified after deposition. Low Eh conditions led to trace-element remobilization. Fe, Mn, V and Mo mobilized, diffusing upward and precipitating upon encountering the oxygenated pore waters required for their precipitation. As different oxygen conditions are required for precipitation of these elements, their concentrations became decoupled, showing peaks at different depths. Major chemical changes also accompanied the diagenetic alteration of glass to smectite. REE, and possibly other associated elements, were significantly depleted during this alteration. Eh and alteration of glass are therefore the main factors controlling the geochemical profiles across the K–T boundary at Blake Nose.

We thank the ODP Leg 171B Shipboard Scientific Party and the crew of the *JOIDES Resolution* for assistance with the samples and data, and the Bremen ODP Core Repository for assistance during the sampling party. One of the authors (F. Martínez-Ruiz) thanks the University of Granada and 'Junta de Andalucía' for financial support for participation on ODP Leg 171B. This work was partially supported by Project PB96-1429 (DGES, MEC, Spain) and Research Group RNM0179 (Junta de Andalucía, Spain). We thank the C. I. C. (University of Granada, Spain) for the use of the analytical facilities. We also thank P. Sánchez-Gómez, I. Nieto and E. Abarca for their help in the laboratory. This paper benefited from the careful revision of C. Koeberl.

References

ALVAREZ, L. W., ALVAREZ, W., ASARD, F. & MICHEL, N. V. 1980. Extraterrestrial cause for Cretaceous/Tertiary extinction. *Science*, **208**, 1095–1108.

ALVAREZ, W., CLAEYS, P. & KIEFFER, S. 1995. Emplacement of Cretaceous–Tertiary boundary shocked quartz from Chicxulub crater. *Science*, **269**, 930–935.

BHANDARI, N., SHUKLA, P. N. & CASTAGNOLI, G. C. 1993. Geochemistry of some K–T sections in India. *Palaeogeography, Palaeoclimatology, Palaeoecology*, **104**, 199–211.

BOHOR, B. F., FOORD, E. E. & GANAPATHY, R. 1986. Magnesioferrite from the Cretaceous–Tertiary boundary, Caravaca, Spain. *Earth and Planetary Science Letters*, **81**, 57–66.

BRALOWER, T. J., PAULL, C. K. & LECKIE, R. M. 1998. The Cretaceous–Tertiary boundary cocktail: Chicxulub impact triggers margin collapse and extensive sediment gravity flows. *Geology*, **26**, 331–334.

DYMOND, J., SUESS, E. & LYLE, M. 1992. Barium in deep-sea sediment: a geochemical proxy for palaeoproductivity. *Palaeoceanography*, **7**, 163–181.

GOLDBERG, E. D. & ARRHENIUS, G. 1958. Chemistry of Pacific pelagic sediments. *Geochimica et Cosmochimica Acta*, **13**, 153–212.

HILDEBRAND, A. R., PENFIELD, G. T., KRING, D. A. *et al.* 1991. Chicxulub crater: a possible Cretaceous/Tertiary boundary impact crater on the Yucatan Peninsula, Mexico. *Geology*, **19**, 867–871.

IZETT, G. A. 1991. Tektites in Cretaceous–Tertiary boundary rocks on Haiti and their bearing on the Alvarez impact extinction hypothesis. *Journal of Geophysical Research*, **96**, 20879–20905.

JONES, B. & MANNING, D. A. C. 1994. Comparison of geochemical indices used for the interpretation of palaeoredox conditions in ancient mudstones. *Chemical Geology*, **111**, 111–129.

KELLER, G., MACLEOD, N., LYONS, J. B. & OFFICER, C. B. 1993. Is there evidence for Cretaceous–Tertiary boundary age deep water deposits in the Caribbean and Gulf of Mexico? *Geology*, **21**, 776–780.

KLAUS, A., NORRIS, R. D., KROON, D. & SMIT, J. 2000. Impact-induced mass wasting at the K–T boundary: Blake Nose, western North Atlantic. *Geology*, **28**, 319–322.

KLAVER, G. T., VAN KEMPEN, T. M. G., BIANCHI, F. R. & VAN DER GAAST, S. J. 1987. Green spherules as indicators of the Cretaceous/Tertiary boundary in Deep Sea Drilling Project Hole 603B. *In*: VAN HINTE, J. E., WISE, S. W., Jr *et al.* (eds). *Initial Reports of the Deep Sea Drilling Project*, **93**. US Government Printing Office, Washington, DC, 1039–1056.

KOEBERL, C. & SIGURDSSON, H. 1992. Geochemistry of impact glasses from the K–T boundary in Haiti: relation to smectites and a new type of glass. *Geochimica et Cosmochimica Acta*, **56**, 2113–2129.

KYTE, F. T., SMIT, J. & WASSON, J. 1985. Siderophile interelement variations in the Cretaceous–Tertiary boundary sediments from Caravaca, Spain. *Earth and Planetary Science Letters*, **73**, 183–195.

KYTE, F. T., ZHOU, Z. & WASSON, J. 1980. Siderophile-enriched sediments from the Cretaceous–Tertiary boundary. *Nature*, **288**, 651–656.

MARTÍNEZ-RUIZ, F., ORTEGA-HUERTAS, M. & PALOMO, I. 2000. Climate, tectonics and meteoritic impact expressed by clay mineral sedimentation across the Cretaceous–Tertiary boundary at Blake Nose, Northwestern Atlantic. *Clay Minerals*, in press.

MARTÍNEZ-RUIZ, F., ORTEGA-HUERTAS, M., PALOMO, I. & BARBIERI, M. 1992. The geochemistry and mineralogy of the Cretaceous–Tertiary boundary at Agost (southeast Spain). *Chemical Geology*, **95**, 265–281.

MARTÍNEZ-RUIZ, F., ORTEGA-HUERTAS, M., PALOMO-DELGADO, I. & SMIT, J. 2001. K–T boundary spherules from Blake Nose (ODP Leg 171B) as a record of the Chicxulub ejecta deposits. *This volume*.

MELOSH, H. J. & VICKERY, A. M. 1991. Melt droplet formation in energetic impact events. *Nature*, **350**, 494–496.

NORRIS, R. D., HUBER, B. T. & SELF-TRAIL, J. 1999. Synchroneity of the K–T oceanic mass extinction and meteorite impact: Blake Nose, Western North Atlantic. *Geology*, **27**, 419–422.

NORRIS, R. D., KROON, D., KLAUS, A. *et al.* (eds) 1998. *Proceedings of the Ocean Drilling Program, Initial Reports*, **171B**. Ocean Drilling Program, College Station, TX.

OLSSON, R. K., MILLER, K. G., BROWNING, J. V., HABIB, D. & SUGARMAN, P. J. 1997. Ejecta layer at the Cretaceous–Tertiary boundary, Bass River, New Jersey (Ocean Drilling Program Leg 174AX). *Geology*, **25**, 759–762.

PAYTAN, A. 1995. *Marine barite, a recorder of oceanic chemistry, productivity, and circulation*. Ph.D thesis, Scripps Institute of Oceanography, University of California, San Diego.

PAYTAN, A., KASTNER, M., MARTIN, E. D., MACDOUGALL, J. D. & HERBERT, T. 1993. Marine barite as monitor of seawater strontium isotope composition. *Nature*, **366**, 445–449.

PIERAZZO, E. & MELOSH, J. H. 1999. Hydrocode modeling of Chicxulub as an oblique impact event. *Earth and Planetary Science Letters*, **165**, 163–176.

POLLASTRO, R. M. & BOHOR, B. F. 1993. Origin and clay-mineral genesis of the Cretaceous/Tertiary boundary unit, Western Interior of North America. *Clays and Clay Minerals*, **41**, 7–25.

RENARD, M. 1986. Pelagic carbonate chemostratigraphy (Sr, Mg, ^{18}O, ^{13}C). *Marine Micropalaeontology*, **10**, 117–164.

ROCCHIA, R., BOCLET, D., BONTÉ, Ph. *et al.* 1990. The Cretaceous–Tertiary boundary at Gubbio revisited: vertical extent of the Ir anomaly. *Earth and Planetary Science Letters*, **99**, 206–219.

SCHMITZ, B. 1985. Metals precipitation in the Cretaceous–Tertiary boundary clay at Stevns Klint, Denmark. *Geochimica et Cosmochimica Acta*, **49**, 2361–2370.

SCHMITZ, B. 1987. Barium, equatorial high productivity, and the northward wandering of the Indian continent. *Palaeoceanography*, **2**, 63–78.

SHARPTON, V. L., BURKE, K., CAMARGO, A. *et al.* 1993. Chicxulub multiring impact basin: size and other characteristics derived from gravity analysis. *Science*, **261**, 1564–1567.

SMIT, J. 1990. Meteorite impact, extinctions and the Cretaceous–Tertiary boundary. *Geologie en Mijnbouw*, **69**, 187–204.

SMIT, J. 1999. The global stratigraphy of the Cretaceous–Tertiary boundary impact ejecta. *Annual Reviews of Earth and Planetary Sciences*, **27**, 75–113.

SMIT, J., MONTANARI, A., SWINBURNE, N. H. M. *et al.* 1992. Tektite-bearing, deep-water clastic unit at the Cretaceous–Tertiary boundary in northeastern Mexico. *Geology*, **20**, 99–103.

SMIT, J., ROCCHIA, R., ROBIN, E. & ODP Leg 171B Shipboard Party. 1997. Preliminary iridium analyses from a graded spherule layer at the K–T boundary and late Eocene ejecta from ODP Sites 1049, 1052, 1053, Blake Nose, Florida. *Geological Society of America, Abstracts with Programs*, **29**, A141.

SPEED, C. D. & KROON, D. 2000. Inorganic geochemistry and mineralogy of the Cretaceous–Tertiary boundary section in Hole 1049C. *In*: KROON, D., NORRIS, R. D. & KLAUS, A. (eds). *Ocean Drilling Program, Scientific Results*, **171B**. Ocean Drilling Program, College Station, TX, 1–26.

STRONG, C. P., BROOKS, R. R., WILSON, S. M. *et al.* 1987. A new Cretaceous–Tertiary boundary site at Flasboumern River, New Zealand: biostratigraphy and geochemistry. *Geochimica et Cosmochimica Acta*, **51**, 2769–2777.

WIGNALL, P. B. & MYERS, K. J. 1988. Interpreting the benthic oxygen levels in mudrocks: a new approach. *Geology*, **16**, 452–455.

ZACHOS, J. C., ARTHUR, M. A. & DEAN, W. E. 1989. Geochemical and palaeoenvironmental variations across the Cretaceous/Tertiary boundary. *Palaeogeography, Palaeoclimatology, Palaeoecology*, **69**, 245–266.